CORRECTION OF CHANDRAYAAN-1 M³ LUNAR HYPERSPECTRAL IMAGE DATA WITH RESPECT TO LOCAL TOPOGRAPHY. C. Wöhler[1] and A. Grumpe[1], [1]Image Analysis Group, TU Dortmund University, D–44227 Dortmund, Germany; {christian.woehler | arne.grumpe}@tu-dortmund.de

Introduction: Lunar multispectral and hyperspectral image data are typically represented in terms of spectral ratios [1] or specific features of an absorption trough, such as its absorption wavelength, absorption depth, and full width at half maximum (FWHM) [2]. It is commonly known that small-scale variations of illumination due to local topography lead to spurious variations of spectral ratios and the inferred FeO and TiO_2 content of the lunar soil [3, 4]. In this study we propose an empirical method to correct Chandrayaan-1 M³ hyperspectral image data with respect to the local topography based on a digital elevation model (DEM) of high lateral resolution constructed with the photometric method described in [5, 6].

Calibration Method: For our hyperspectral data analysis we utilise 85-channel hyperspectral radiance image data acquired with the Chandrayaan-1 M³ instrument (http://m3.jpl.nasa.gov/m3data.html). Due to poor calibration, we omit channels 1–5 (cf. [7]) and 85. The remaining channels 6–84 cover the wavelength range from 661 to 2936 nm. The lateral image resolution typically corresponds to 140 m/pixel.

Thermal correction. We applied a thermal correction to the radiance spectra by modeling them as being composed of a scaled standard linear reflectance spectrum inferred from returned lunar sample no. 62231 and a black body emission spectrum in the wavelength range 2377–2936 nm, thus estimating the temperature of the black body. Division by the known solar irradiance then yields the reflectance spectrum corrected for thermal emission.

Normalisation to standard geometry. Relying on the image-based photometric approach introduced in [5, 6], a DEM of the examined region is constructed, which has a lateral resolution that comes close to that of the M³ images. Based on this DEM and the known direction to the sun, the topography-dependent incidence and emission angle are computed for each pixel. Channel-wise maps of the locally variable single-scattering albedo according to the Hapke IMSA [8, 9, 10] or AMSA [11] model are computed based on the DEM, thus allowing to infer pixel-wise reflectance spectra for a standard geometry of 30° incidence angle, 0° emission angle, and 30° phase angle.

Extraction of spectral features. The absorption wavelength λ_{abs}, the relative absorption depth δ, and the full width at half maximum (FWHM) of the ferrous absorption trough around 1000 nm are extracted from the normalised continuum-removed spectra after division by the continuum, which is approximated by the straight line between the reflectance values at 701 and 1249 nm. It is straighforward to determine further features such as spectral ratios or integrated band depths.

Empirical topography correction. To obtain a topography correction of the examined region, a small crater is selected for which it can be assumed that all pixels on the inclined inner wall intrinsically have identical spectral properties. The average spectrum S_λ of all inclined pixels in this reference region is assumed to be the "true" spectrum, and all observed spectral variations across the inner wall are attributed to local topography. The normalised ratio spectrum of pixel (x,y) then corresponds to

$$Q_\lambda(x,y) = \left[R_\lambda(x,y)/S_\lambda\right] / \left\langle R_\lambda(x,y)/S_\lambda \right\rangle_\lambda$$

with $\langle \ldots \rangle_\lambda$ as the average over all wavelengths. A principal component analysis (PCA) is computed for all normalised ratio spectra of the reference region, and a polynomial function of 2nd order in the surface slope angle and 8th order in the azimuth angle of the surface normal is fitted to the resulting pixel-wise PCA coefficients, where only the coefficients corresponding to the four most dominant PCA components are regarded. The PCA coefficients are then computed for the complete examined region based on the fitted polynomial and the surface normals inferred from the DEM, and the pixel spectra are corrected accordingly.

Results: Figs. 1–3 show uncorrected and corrected maps of spectral features extracted from M³ data. Cold colours correspond to low values and warm colours to high values. Very dark pixels are masked out in black since they correspond to shadowed or strongly shaded areas. The topographic effects are most strongly apparent for the absorption wavelength λ_{abs}, which is an important diagnostic feature as it is an indicator of the Ca content of pyroxene [12] and may thus allow to distinguish between orthopyroxene and clinopyroxene.

Fig. 1 shows the spectral features before and after correction for a 30 x 23 km² region on the floor of the crater Huggins, including the crater Huggins A. Fig. 2 shows the uncorrected and corrected absorption wavelength λ_{abs} for a 30 x 25 km² region immediately south of the crater Huggins where many small craters are located, all of which show topography-dependent anomalies of λ_{abs} prior to the correction. The central peaks of Bullialdus shown in Fig. 3 (size of the region: 22 x 31 km²) are known to consist of noritic material [13]

and therefore exhibit significantly lower values of λ_{abs} than the surrounding crater floor [2]. Without correction, the southern flanks of the central peaks are associated with systematically higher values of λ_{abs} than the northern flanks. This spurious asymmetry is eliminated by the topography correction.

Conclusion: We have presented an empirical, PCA-based method for correcting M³ hyperspectral image data with respect to the influence of small-scale local topography based on local DEMs of high lateral resolution. Our results show that the proposed method is able to strongly attenuate the initially significant influence of local topography on the spectral features.

References: [1] Lucey P. G., et al. (2000) *J. Geophys. Res. 105 (E8)*, 20297–20306. [2] Wöhler C. et al. (2011) *PSS 59*, 92–110. [3] Jolliff B. L. (1999) *JGR Planets 104*, 14123–14148. [4] Cahill J. T. et al. (2007) *LPSC XXXVIII*, abstract #1967. [5] Grumpe A. et al. (2011) *LPSC XXXXII*, abstract #1478. [6] Grumpe A. and Wöhler C. (2011) *Proc. 7th Int. Symp. Image and Signal Processing and Analysis*, 609–614. [7] Isaacson P. et al. (2011) *http://pds-imaging.jpl.nasa.gov/documentation/Isaacson_M3DataTutorial_EPSCDPS 2011_Final.pdf*. [8] Hapke B. W. (1981) *J. Geophys. Res. 86*, 3039–3054. [9] Hapke B. W. (1984) *Icarus 59*, 41–59. [10] Hapke B. W. (1986) *Icarus 67*, 264–280. [11] Hapke B. W. (2002) *Icarus 157*, 523–534. [12] Matsunaga T. et al. (2008) *Geophys. Res. Lett. 35*, L23201. [13] Tompkins S. et al. (1994) *Icarus 110(2)*, 261–274.

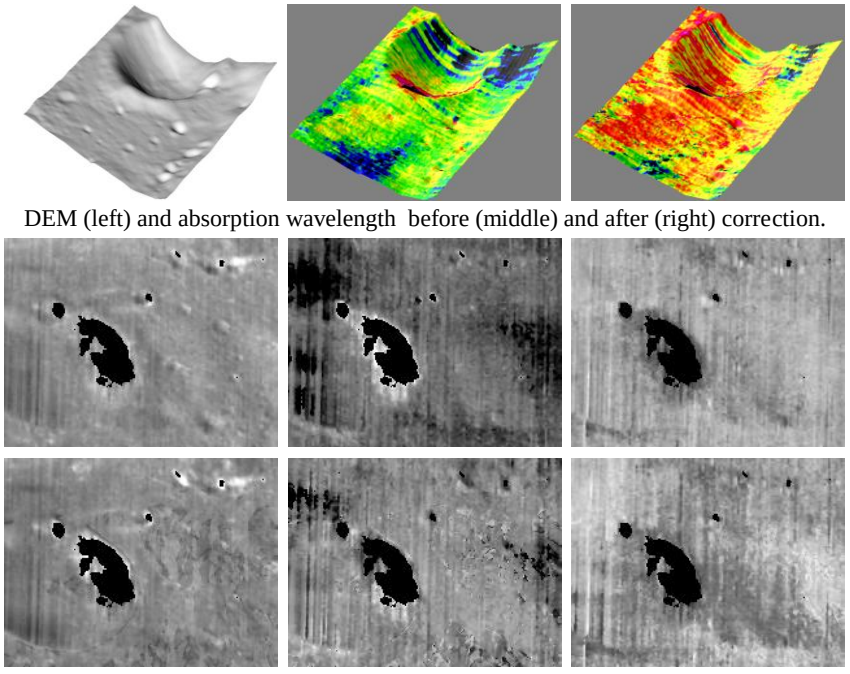

Fig. 1: Spectral feature maps of the region around the crater Huggins A. Top: DEM and absorption wavelength (range: 880–1000 nm). Bottom: Band depth (left), λ_{abs} (middle), and FWHM (right) before (upper row) and after correction (lower row). The uncorrected band depth and λ_{abs} values show strong correlations with surface slope, especially for small craters and the western inner wall of Huggins A.

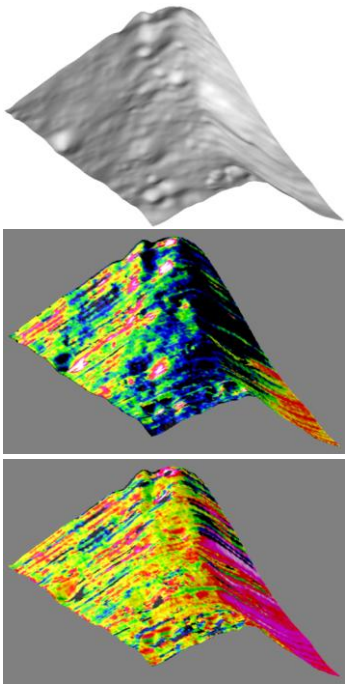

Fig. 2: DEM (top) and absorption wavelength before (middle) and after (bottom) topographic correction for a region south of the crater Huggins. Wavelength range: 880–1000 nm.

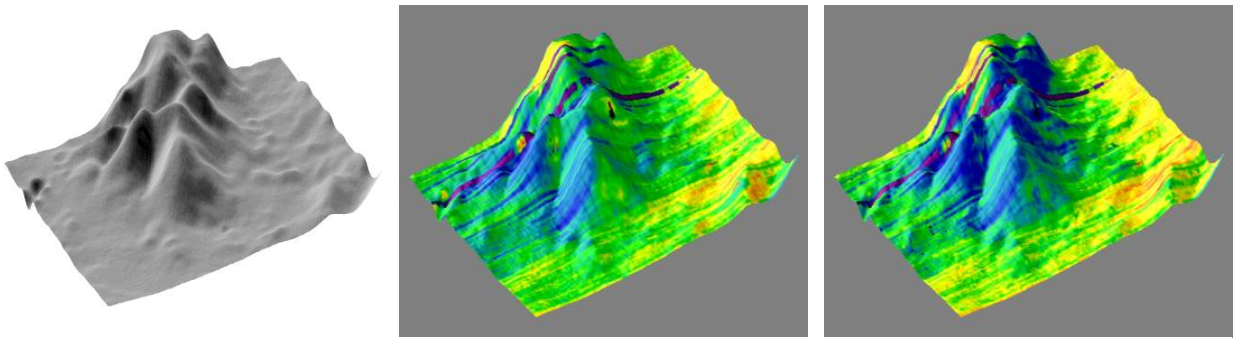

Fig. 3: DEM (left) and absorption wavelength before (middle) and after (right) topographic correction for the central peaks of the crater Bullialdus. Wavelength range: 880–1000 nm.